Molecular Dynamics Study of Selective Adsorption of PCB on Activated Carbon

Bjørnar Jensen[a,*], Tatiana Kuznetsova[a], Bjørn Kvamme[a], Åge Oterhals[b]

[a] *Institute of Physics and Technology, University of Bergen, Allégaten 55, 5020 Bergen, Norway*

[b] *Nofima Ingrediens, Kjerreidviken 16, 5141 Fyllingsdalen, Norway*

Abstract

The selectivity of PCB adsorption from fish oil onto activated carbon (AC) was investigated by means of molecular dynamics to determine the importance of molecular planarity. PCB congeners 77 and 118 were selected for comparison purposes due to pronounced differences in mean adsorption efficiency and molecular geometry; triolein, a triacylglycerol of oleic acid (C18:1), was used as the representative fish oil component. Graphitic carbon structure was set up to serve as activated carbon model. Molecular force fields employed in the simulations combined short-range parameters from the OPLS with partial atomic charges obtained via quantum chemical calculations using DFT/B3LYP/6-31**G+ and Solvation Model 6. We modified the dihedral angle potential between the PCB aromatic rings and applied Schrödinger's Jaguar package to evaluate the required force field constants. Our complete system comprised a number of PCB molecules dissolved in triacylglycerol that overlaid and filled the pores of an AC structure. The production run of 4 ns provided strong indications that smaller pores will be conductive to better selectivity though also resulted in certain doubts concerning the the estimation and assignment of partial atomic charges on the activated carbon. The majority of PCB molecules trapped in pores were attached via cl–AC "bonding", leaving the main part of the PCB molecule free to interact with triolein. The cl–AC adsorption energy was found to surpass the energy criteria conventionally used for hydrogen bonds. Planar orientation assumed by a PCB molecule in a very energetically favored position on

*Corresponding author. Tel.: +47 555 82877

Email address: Bjornar.Jensen@ift.uib.no (Bjørnar Jensen)

top of the graphite sheet clearly supported the π-cloud overlap hypothesis.

Keywords: Molecular dynamics, activated carbon, PCB, adsorption

1. Introduction

Polychlorinated polychlorinated biphenyls (PCB) together with dibenzo-p-dioxins and dibenzofurans (PCDD/F) are classified as persistent organic pollutants (POPs), known to bioaccumulate in the food chain [1]. Fish oil produced from pelagic fish and their by-products is used as polyunsaturated ω-3 fatty acid source in compounded feeds. High inclusion levels make it the main POP contributor in Atlantic salmon feed [1–3]. The level of POPs in North European fish stocks are generally higher than in the South Pacific ones, putting the fish-processing industry in the region at a distinct disadvantage since parts of their fish oil and fishmeal products need to be purified to comply with the maximum permitted levels [1, 4]. The POPs level in produced fish oil will depend on the pollution status in the respective fishing areas and seasonal variation in the fat content of the fish [1, 4]. POPs are lipophilic compounds and accumulate in the fatty tissue of living organisms. The lowest level of fat, i.e. the highest concentration of POPs in the extracted fish oil, occurs right after the spawning period. To remain competitive, North European fish oil and fish meal industry needs a cost-effective way to reduce the PCB levels to comply with requirements set by the European legislation.

It has been shown in previous research [1] that adsorption onto activated carbon is a viable option for PCDD/F removal, but is much less effective when it comes to PCB reduction. A wide variation in the efficiency of the activated carbon adsorption process for different PCB congeners has also been observed in a process optimization study by Oterhals et al. based on alkali-refined and bleached fish oil. PCB congener 77 — 3,3',4,4'-tetrachlorobiphenyl — had a mean adsorption efficiency of 74.7%, while PCB congener 118 — 2,3',4,4',5-pentachlorobiphenyl — only 10.1%. Both of these congeners are classified as dioxin-like PCB (DL-PCB) pollutants but differ in a significant aspect. PCB congener 118 is characterized by a mono-ortho substitution, while PCB congener 77 has no substitutions in any ortho positions. This observation led Oterhals et al. to suggest that adsorption of PCB onto activated carbon may be dependent on the co-planar configuration of the molecule. The hypothesis is supported by research findings from other groups [5–8].

Activated carbon has slit pores dominated by micropores <2 nm [9]. The

microstructure consists of a heterogenic network of defective hexagonal carbon layer planes of typically 5 nm width, cross-linked by aliphatic bridging groups. Functional groups (e.g., C-OH, C=O) can be introduced during the activation process by reaction with oxidizing gasses like H_2O and CO_2 [9]. Such functional groups have an important influence on adsorption properties [10]. According to the hypothesis put forward by Oterhals et al., the PCB congener 118 with its mono-ortho substitution will be unlikely to assume a planar configuration and consequently have greater difficulties in entering and becoming trapped in the micropores of the activated carbon. Another hypothesis proposed that molecules with a planar conformation will create a favorable π-cloud overlap between the aromatic rings in the PCB molecules and the hexagonal structure in activated carbon and other carbonic materials [7, 11]. However, Jonker and Koelmans were unable to verify such contributions based on their results. Jonker and Koelmans went on to suggest that pore sorption will be the most important factor for PCB adsorption mechanism. This work aimed to investigate this hypothesis by means of molecular dynamics simulation and thus we focused on a structure that mimics the pores of the activated carbon.

Graphite was chosen as the model for activated carbon, while triolein, a triacylglycerol of oleic acid (C18:1), one of the major fatty acids in fish oil [12], represented the solvent. Based on their large difference in adsorption efficiencies, two PCB congeners 77 and 118 were selected from Oterhals et al.

2. Computational Methods

2.1. Force Field

Optimized Potential for Liquid Simulations (OPLS) force field by William L. Jorgensen [13–21] was primarily used to parameterize the models. The OPLS splits the energy contributions into two distinct classes, bonded and non-bonded contributions. Bonded contributions consist of bond stretching, angle bending and twisting of dihedral angles, while non-bonded contributions are van der Waals forces and electrostatic forces modeled by Lennard-Jones 12-6 potential and Coulomb's law, respectively.

The potential for bond stretching is a harmonic potential and given in equation 1.

$$E_{bond} = k_s \times (R - R_{eq})^2 \tag{1}$$

where E_{bond} is the energy; k_s is the force constant; R is the bond length and R_{eq} is the equilibrium bond length specified by the force field.

Any deviation from the bond length will give a positive energy contribution, and thus a force will try to counteract the stretching or compression of the bond. The potential for bending of angles is also harmonic and shown in equation 2.

$$E_{angle} = k_b \times (\theta - \theta_{eq})^2 \tag{2}$$

where θ and θ_{eq} is the current and equilibrium angles in degrees, respectively. k_b is the force constant. For the dihedral angles the potential is described by a Fourier series in the following manner (eq. 3).

$$\begin{aligned} E_{dihedral} &= \frac{V_1}{2} \times [1 + \cos\phi] + \frac{V_2}{2} \times [1 - \cos 2\phi] \\ &+ \frac{V_3}{2} \times [1 + \cos 3\phi] + \frac{V_4}{2} \times [1 + \cos 4\phi] \end{aligned} \tag{3}$$

where V_1, V_2, V_3 and V_4 is the Fourier coefficient, analogue to the force constants in equations 1 and 2; ϕ is the dihedral angle. The equilibrium angle is given by the minimum value of the Fourier series. Furthermore, the non-bonded contributions are given by (eq. 4):

$$E_{ab} = \sum_{i}^{on\ a} \sum_{j}^{on\ b} \left[\frac{q_i q_j e^2}{r_{ij}} + 4\varepsilon_{ij} \left(\frac{\sigma_{ij}^{12}}{r_{ij}^{12}} - \frac{\sigma_{ij}^{6}}{r_{ij}^{6}} \right) \right] f_{ij} \tag{4}$$

where a and b are different atoms; q_i and q_j are partial atomic charges for atoms a and b; e is the elementary charge; r_{ij} is distance between a and b; ε_{ij} is the well depth; σ_{ij} is a distance parameter and f_{ij} is a scaling parameter which has the value of 0.5 if a and b are connected by bonds via 2 other atoms (1,4) or 1.0 if they are further separated.

2.2. Fitting of torsional potential for PCB

The dihedral angle between the benzene rings in PCB congeners will be of significant importance for the hypothesis under investigation since it determines the planar configuration of the molecule. We believed this dihedral warranted a more thorough analysis via a rigid coordinate scan carried out by Schrödingers Jaguar package [22]. We used density functional theory (DFT) with B3LYP functional [23, 24] and a Pople style 6–31**g+ basis set. The

relative coordinates of all other atoms were kept constant while the dihedral angle around $C_1 - C_1'$ varied within the 0–360 degree range. The scan yielded the energy profile as a function of dihedral angle. This profile was then zero-shifted and compared to energies predicted by the OPLS-style dihedral angle that used biphenyl parameters.

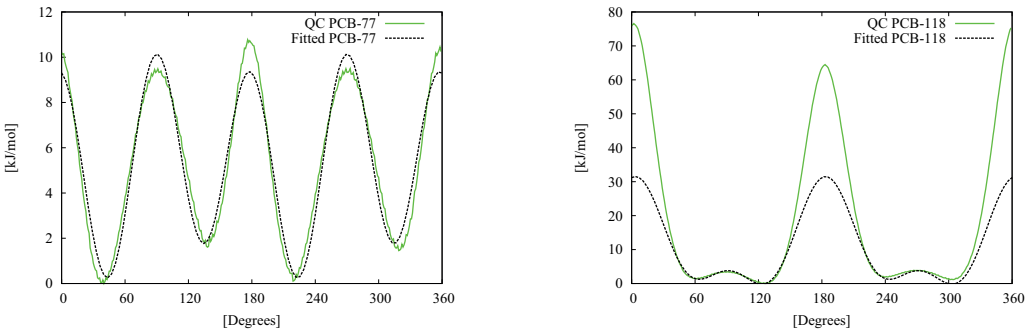

Figure 1: Dihedral energies for PCB congener 77 (left) and congener 118 (right). Solid green lines for energies obtained from quantum chemical methods, dashed blue lines are energy from potential used in simulation by fitting parameters in equation 5 to the QC energies.

The QC-derived dihedral energy profile deviated to a significant degree from the OPLS one in case of both PCB congeners. Figure 1 make it obvious that the two dihedral angles cannot, as they are in OPLS, be described by the same parameter set. Achieving an agreement between the QC results and the OPLS potential demanded some modifications to the functional form of the dihedral potential itself. The new potential was least-squares fitted to minimize the deviations from the energy profile. Due to the scanning procedure potentially overestimating the effect of rotations, this approach did not work very well for the PCB congener 118 which exhibited a very high rotational barrier and led us to focus the fit on the region containing the local and global minima instead of the whole plot. Though the fitted potential failed to replicate the global maxima for PCB congener 118, this did not appear to affect the accuracy of the potential to any significant degree and the correct description of local and global minima was deemed to be of greater importance. The new potential used for the $C_1 - C_1'$ dihedral is presented in 5:

$$E_{dihedral} = \frac{V_1}{2} \times [1 + \cos(2\phi + f_1)] + \frac{V_2}{2} \times [1 - \cos(2\phi + f_2)]$$

Table 1: Force field parameters for phenyl-phenyl dihedral angle in PCB congener 77 and congener 118. Fitted with method of least squares to QC energy calculations. V_1, V_2, V_3 in $kJ\ mol^{-1}$, f_1, f_2 and f_3 in *degrees*.

PCB Congener	V_1	f_1	V_2	f_2	V_3	f_3
3,3',4,4'	0.144	26.288	0.870	-51.255	4.359	4.305
2,3',4,4',5	9.009	-13.929	-4.961	-0.778	6.800	-11.720

$$+ \quad \frac{V_3}{2} \times [1 + \cos(4\phi + f_3)] \tag{5}$$

where the only new parameters are $f_x, x = 1 \ldots 3$, phase angles determining the phase shift of the curve. This allows to shift the minima and maxima towards correct positions. We should also note that the multipliers within the cosines has been changed in comparison to those from equation 3 to allow for better fitting to the quantum chemical energies. The parameters in equation 5 for PCB congener 77 and 118 are listed in table 1.

2.3. Obtaining partial atomic charges

To the best of our knowledge, all previous simulations involving activated carbon employed zero partial atomic charges [25, 26]. This approach is quite reasonable for a uniform surface such as the top layer of a graphite sheet, but the influence of pore corners, sheet edges, and other irregularities may lead to polarization and thus non-neutral carbons. Other reported studies that also used zero partial atomic charges for the graphite, accounted for these effects by including active sites like OH– and COOH– groups [27], with the functional groups assigned charges taken from literature.

We deemed it inappropriate to utilize partial atomic charges obtained from vacuum calculations for our particular system. This consideration, together with the lack of certain parameters, ruled out using the OPLS force field charges. An approach utilizing continuum solvent models was chosen to generate partial charges for the triacylglycerol, triolein, and both PCB congeners. We employed DFT with the B3LYP functional and a 6–31**g+ basis set. Solvation Model 6 (SM6) was used as the continuum solvation model [28]. The implementation of this model in Jaguar relies on Charge Model 4 (CM4) [29] to obtain Class IV partial atomic charges for use in the calculation. Mülliken and Löwdin charge models were rejected outright, due to their sensitivity to large basis sets. CM4 utilizes the Redistributed Löwdin Population Analyzes (RLPA) [30] in order to estimate its Class 4 charges

which alleviates, to a certain degree, the problems with Löwdin population analyzes when using large (mainly diffuse) basis sets.

The sheer size of the AC model made it unfeasible to run an all-atom quantum chemical simulation to obtain the partial charges. A smaller model, consisting of 3 layers and 162 carbon atoms in graphitic configuration was used. Furthermore, all attempts to run simulations using SM6 proved to be unsuccessful as the self consistent field failed to converge when continuum medium was added. Consequently, the partial atomic charges had to be obtained by performing a vacuum simulation and applying the electrostatic potential scheme.

The resulting partial atomic charges exhibited a wide variance depending on position. Atoms close to the edge of the model got assigned significant charges, while atoms further away, almost-zero charges. A pattern emerged upon the further study where the partial atomic charges appeared to alternate in polarity and with magnitude of the charges decaying with the distance from the edge. These findings were implemented for the AC model by averaging the partial atomic charges in the same row. This was done for carbon atoms up to the depth of four rows. The averaged charges were then assigned to atoms close to the pore edges of the AC model. All the remaining carbon atoms were assigned a random charge distribution ensuring the electroneutrality of the whole model.

3. Simulation Setup and Software

We used molecular dynamics package MDynaMix version 5.1 by [31]. This package is available as source code at the MDynaMix home page [32]. It has been widely used by our research group. In order to visualize the simulation, as well as generate snapshots of interesting details, Visual Molecular Dynamics (VMD) [33] was used.

The complete simulation system consisted of an activated carbon block and a liquid system containing two PCB congeners, 77 and 118, dissolved in a triacylglycerol, triolein. The system setup was divided into three stages. First, the activated carbon model was inserted into a simulation box, and centered to replicate seamlessly in the x and y directions. Subsequently, a liquid system was put together with x- and y- cell dimensions identical to those of the activated carbon model. The height of the simulation box was, however, significantly higher than required to obtain the target density of 915 $kg\ m^{-3}$. Also, only one third of the molecules for each constituent was

used. This was done to reduce the simulation time needed to compress the system to the target density. As well as to avoid overlaps that can arise when assembling the system and potentially leading to nonphysical lockups and tremendous forces. Only the z distances were scaled between the runs. The system was ran at 2000 K for 20.000 steps (of 0.1 femtoseconds) between the scalings to allow it to settle into a reasonable configuration. During this phase, simple velocity scaling was used to control the temperature. The initial dimensions of the system was (80.814 x 78.580 x 1100.000)Å.

Predominantly, the system was scaled in the z dimension by about 10% each time. In the early stages, it was scaled by 100Å each run until the height reached 700Å, afterwards the scaling was kept at 10% between each run. When the height reached 50Å, it was reduced by 5Å every run until 25Å and then scaled to the target value of 24.260Å to yield the density of 915 $kg\ m^{-3}$. The primary cell was then replicated twice in the z dimension to obtain the desired the volume and number of molecules. This system was simulated for an extended time in order to reduce the memory of initial state. The temperature was then scaled down to 330K, to reproduce the mean experimental temperature used in Oterhals et al. [1].

To complete the system setup, the liquid solution box was placed on top of the activated carbon model, with a 5Å gap to avoid overlaps. A constant external electrostatic potential was applied to force the liquid solution into the pores of the activated carbon. This potential was gradually scaled down to avoid a rapid rebound expansion due to Newton's 3rd law. The activated carbon block was fixed both during system setup and the main simulation run.

The composite system consisted of an activated carbon block with 31.232 carbon atoms, 252 triolein molecules of 167 atoms, and 51 molecules of both 77 and 118 PCB congeners, each comprising 22 atoms. The total number of atoms amounted to 75,560. The time step was set to 1.0 femtoseconds, temperature to 330K. Initially, simple velocity scaling was used to control temperature, Nosé-Hoover thermostat [34–36] with a relaxation time of 50 femtoseconds was switched on as the system stabilized. Periodic boundary conditions in x, y and z dimensions were set to $(80.814 \times 78.580 \times 220.000)$Å. During the entire simulation, from early setup to end of production run, the activated carbon was fixed with no translational or rotational degrees of freedom. Simulations were run in parallel on 256 cores on the Hexagon supercomputer Cray XT4 at the Bergen Center for Computational Sciences. The total run time for the system amounted to 5 months, with the simulation

extending to just over 4 nanosecond.

4. Results and Discussion

4.1. Visual Inspection

At the start of the production run — after the initial setup, compression and down-scaling runs — there were only seven PCB molecules within the pores of the activated carbon. Four of those molecules were PCB congener 77 and the remaining three, PCB congener 118. At the end of the run, the same seven PCB molecules remained in the pores. No new PCB molecules entered the pores, nor did any of the initial seven molecules leave. Given that the total number of PCB molecules amounted to 102, this means that PCB 77 and 118 congeners exhibited quite similar pore trapping efficiency in our simulated system, in stark contrast with their significant experimental selectivity. However, it is hard to draw rigorous conclusions concerning the selectivity from the limited number of trapped PCB molecules due to little statistical significance.

After system initiation described in section 3 and at the start of the production run, a single PCB congener 118 was observed positioned right alongside the pore wall with its aromatic rings flat against the wall. One molecule of PCB congener 77 was also aligned with the pore walls, but located in the middle of the pore and not adsorbed in the same manner as the congener 118 molecule. The other five molecules were all attached to the pore walls via either one or two of their chlorine substitutions. One of these molecules, a PCB congener 77, later positioned itself directly adjacent to the pore wall in a configuration similar to the one of initially adsorbed congener 118 molecule. None of the other PCB molecules was able to assume a similar orientation, and no PCB molecule anchored by its chlorine atoms detached from the pore wall. Nor did any but the already specified molecule come close to aligning with the wall in a planar configuration, either. The PCB congener 77 molecule that remained parallel to the pore wall from the start was unable to move any closer to the wall within the time frame of the simulation. Any movement towards the pore wall was blocked by the hydrocarbon tails of the triolein molecules separating it from the wall.

While apparently being unable unable to tear loose from the walls within the simulation time, some the PCB molecules showed a tendency to diffuse along the wall surface. Those molecules tended to remain at the same pore depth, neither moving deeper nor leaving the pore. This observation does,

however, raise the question of what will happen when the solvent molecules are partially replaced by gas, for instance when the activated carbon is separated from the fish oil in an experimental setting. Would the PCB molecules attached via chlorine atoms remain loosely anchored, would they adsorb onto the pore wall, or simply detach and leave the pore with the solvent?

The results of our simulation did not support any significant selectivity for congener 77 over congener 118 as seen in experiments. Both pores in our activated carbon model were slit pores in the meso-pore range with the width slightly exceeding 20Å. Considering that the gyration radius of PCB congener 77 molecules — with the $C_1 - C_1'$ dihedral angle offsetting the aromatic rings — amounts to just about ∼5.0–5.5Å, it is likely that any selectivity will only reveal itself in much smaller pores. Our calculations indicate that PCB congener 118 will assume a slightly larger conformation with a radius of ∼5.8–6.5Å. This estimate assumes that the dihedral is oscillating around its global minimum and neglecting the fact that the local maximum is only 3–4 $kJ\ mol^{-1}$ high, and this barrier might not be enough to stop the molecule from switching back and forth between the global and local minimum of the dihedral angle. Thus if a PCB congener 118 molecule enters a pore narrower than ∼7.5Å, it will loose the ability to shift the dihedral angle between these two minima. This loss of rotational freedom will result in entropy penalty. It should be noted that Jonker and Koelmans [7] found indications in their work that for PCB adsorption the average pore distribution had a strong positive correlation with the distribution coefficients. For both PCB congener 77 and 118 activated carbon had the largest distribution coefficient in their study, and also the lowest average pore diameter with 3.0 nm. Activated carbon also had the largest total pore volume and specific surface area. This, along with the discussion above, is in our opinion indicative that smaller pores should be more thoroughly investigated.

However, the large size of solvent molecules make even their tightest conformation experience significant interactions with the pore walls. Thus, in contrast with true bulk solution, the solvent's internal energy will be affected by the activated carbon. One would expect, for instance, that their range of molecular movement will be restricted compared to true bulk solution leading entropy decrease in comparison to bulk. From a thermodynamic point of view, this could mean that chemical potential of molecules within the pores will deviate from its bulk value, which will also impact the adsorption process. In view of this, it is not only important to study smaller pores, but also to attain a comparative study of larger pores. While the adsorption is onto

the activated carbon, one should not neglect the impact and interactions of and with the solvent.

Another issue to consider is that a larger pore with a true bulk solution in the middle might have a larger mass flow between the pore and the bulk outside. The higher flux will facilitate transport of PCB molecules into the pore, and thus provide more opportunities for pore adsorption. Additionally, PCB congener 118 will be less constrained in a larger pore, but the entropy penalty will arise again as it moves from the bulk in the middle into the boundary layer close to activated carbon. An interesting model for such a system would be a varying-width slit pore with the top diameter > 50Å that narrows down to ~ 5Å. Such a model is expected to shed some more light on the effects discussed here.

4.2. Impact of partial atomic charges

The partial atomic charges of the activated carbon atoms were obtained by averaging the electrostatic potential (ESP) from quantum chemical vacuum simulation. This approach to estimating charges, together with the fact that they were not verified against experimental data, made us to put the AC charges under additional scrutiny. This is especially relevant given that a number of phenomena observed made during the simulation appeared to be dominated by electrostatics, with the partial atomic on the activated carbon contributing to the effect.

Due to the magnitude of partial atomic charges at the pore edge, the triolein solvent molecules tended to orient their polar heads towards the edges (figure 2). As shown in the right part of figure 2 the polar groups in triolein is mainly concentrated over the charged regions of the activated carbon. The more neutrally charged regions of activated carbon has a much higher concentration of non-polar hydrocarbon tails. This orientation led to a clear pattern in the positioning of the head groups. Furthermore, the enhanced concentration of polar head groups has resulted in a surfactant behavior of the solvent, so that the more polar groups were oriented towards the pore edges both close to the pore and further away. This led to a micelle-like formations, with the polar groups in the middle of the bulk solvent and the non-polar hydrocarbon tails pointing outwards, however not quite as structured as regular micelles.

Since PCBs are known to be lipophilic and mostly non-polar, it was no surprise to find that the PCB molecules concentrated among the hydrocarbon tails. The polar groups were attracted to the pore edges, leading to a visible

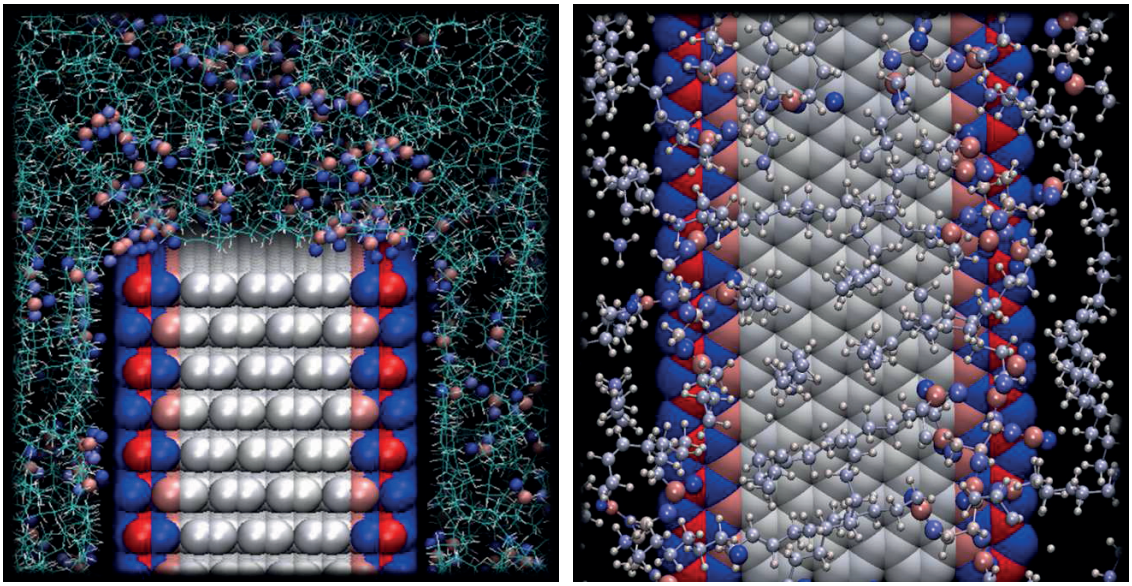

Figure 2: Charge distribution on edges of pores in activated carbon model, blue color indicated negatively charged atoms; red color indicate positively charges regions while white indicate neutral. Note the concentration of polar heads in triolein close to the pores. Also note the relative lack of polar groups in top left and top right corner of the leftmost figure, above the pores themselves. On the figure to the right the high concentration of polar groups over the charged pore edges are quite evident.

high concentration of hydrocarbon tails above the pores themselves and on the outskirts of the liquid solution. A visually high concentration of PCB molecules were observed in the outskirts of the liquid solution, but not so much over the pores.

It also became evident when observing the system that the liquid solution, which started out as a relatively evenly spread film, congregated to a drop-like formation on top of the activated carbon block. This behavior together with the enhanced concentration of the polar heads had a detrimental effect on the simulation. The amount of molecules in the liquid phase was estimated to fill the pores and add a layer extending 20Å above the activated carbon. However, the liquid layer peak extended to more than 120Å above the AC block at end of simulation. This fact may again to some degree be explained by the high partial atomic charges. Another plausible explanation for this phenomenon can be influence of surface roughness. Several studies have

shown that thin films have a tendency to rupture or break up on chemically or physically heterogenous surfaces [37, 38]. We are still not certain, at this time, whether this truly reflects the real behavior or is an artefact of artificially high partial charges on the activated carbon. Additional simulations on a system with carbon surface roughness could shed light on the impact of microscopic roughness on structuring and adsorption. However, the behavior does emphasize the need for a more thorough investigation and likely a better scheme for determination and assignment of partial charges for the activated carbon.

4.3. Interaction Energies

Since the majority of PCB molecules in the pores did not adsorb, nor showed any inclination to do so, a further look into the interaction energies were deemed necessary. One of the hypotheses was that a flat orientation towards the activated carbon would lead to a more favorable interaction energy. According to this working hypothesis the PCB molecules should for the majority, and given enough time, obtain this orientation. However, the observations indicated otherwise.

When examining the chlorine-attached PCB molecules more closely and more specifically estimating the interaction energy for the chlorine-AC interaction for one of the molecules it is observed that the interaction energy in this case was $-14.70\ kJ\ mol^{-1}$. The contribution from electrostatic interaction was $-9.24\ kJ\ mol^{-1}$, while the contribution from Lennard-Jones interaction was $-5.46\ kJ\ mol^{-1}$. In previous studies carried out by other groups the energy criteria for hydrogen bonding were said to be $-10\ kJ\ mol^{-1}$ [39]. By this definition the sum of all chlorine-AC interactions within 10Å is comparable to hydrogen bonding, energetically. Comparing the interaction energy to that of the complete adsorbed PCB 77 molecule makes it evident that under the given circumstances it is seemingly more favorable to only have a chlorine-AC connection. The apparent reason for this is that a single chlorine atom can position itself between three negatively charged activated carbon atoms, and as such coming closer to the second row with positive charged activated carbon atoms. Consequently, the chlorine atom moves mainly along and in-between the graphite sheets. An adsorbed molecule does not have this option due to its size. Hence more chlorine atoms, as well as the mainly negatively charged carbon atoms in the aromatic rings, come into close proximity of the negatively charged activated carbon atoms in the outer row. In summary this results in strong electrostatic repulsion.

Indeed, the electrostatic interaction with the activated carbon is so strong that it leads to a positive interaction energy, thus overcoming the favorable Lennard-Jones interactions. Table 2 show the interaction energies for five PCB molecules of different congener and different positioning. In this table the interaction energies displayed is a sum of the interaction energies between the PCB molecule in question and both activated carbon and triolein. A major point here is that the sum of electrostatic and Lennard-Jones interaction energies from the aforementioned PCB congener 77 molecule with activated carbon is positive. However, due to the favorable interaction with triolein this is not evident in the tabulated data. For the attached PCB congener 77 molecule both the interaction with activated carbon and triolein is negative. Note that for the two PCB molecules adsorbed to the pore wall, PCB congener 118 has the overall lowest interaction energy. While PCB congener 77 has a lower Lennard-Jones interaction energy with AC, the corresponding electrostatic interactions with AC are almost 30 times stronger and more favorable for PCB congener 118.

Table 2: Interaction energies in $kJ\ mol^{-1}$ for PCB molecules. Pore indicates molecules adsorbed to pore wall, top indicates molecule adsorbed to the top of a graphite sheet and attached indicates molecules which only have one or two of their chlorine substitutions pointing towards the pore wall. All values are time averages over the same 12.45 picoseconds and from the very end of simulation (4.1 nanoseconds)

PCB	Placement	*Lennard-Jones*	*Electrostatic*	*Total*
PCB 77	Pore	-151.864	-1.169	-153.034
PCB 118	Pore	-141.686	-30.706	-172.392
PCB 118	Top	-187.834	24.186	-163.648
PCB 77	Attached	-131.038	-64.204	-195.242
PCB 118	Attached	-153.685	-102.873	-256.559

With this in mind, it is more understandable that the remaining PCB molecules did not arrange themselves flat against the pore wall. It is our belief that the regularity of the pore wall may be the deciding factor in making this orientation quite unfavorable for the PCB molecules. Wall defects, with some negative outer carbons removed and inner positive ones exposed, may result in electrostatic interaction becoming more favorable for the planar conformation. What is clear is that while we do have a small indication that there are more PCB 77 molecules in the pore, the interaction energies seems to directly contradict experimental results. Some of this, as mentioned

above, may be due to the total lack of defects in the pore walls. However, we also suspect that we overestimated the magnitude of partial atomic charges and distributed them too uniformly.

As mentioned in the introduction, some published research suggest that selectivity displayed by activated carbon does not really depend on the existence of pores but rather on planar molecules finding it easier to achieve a beneficial orientation with the hexagonal structure of activated carbon. Thus the selectivity will be more affected by the available specific surface area [7, 11]. The course of our simulation saw only one molecule adsorbed on the top of the activated carbon block. This was a congener 118 molecule (figure 3) which had its aromatic ring with three chlorine substitutions flat against the surface, and hydrogens in the other aromatic ring pointing downwards. This molecule adsorbed rather close to the edge of a pore, where the partial atomic charges on the activated carbon model are dominant.

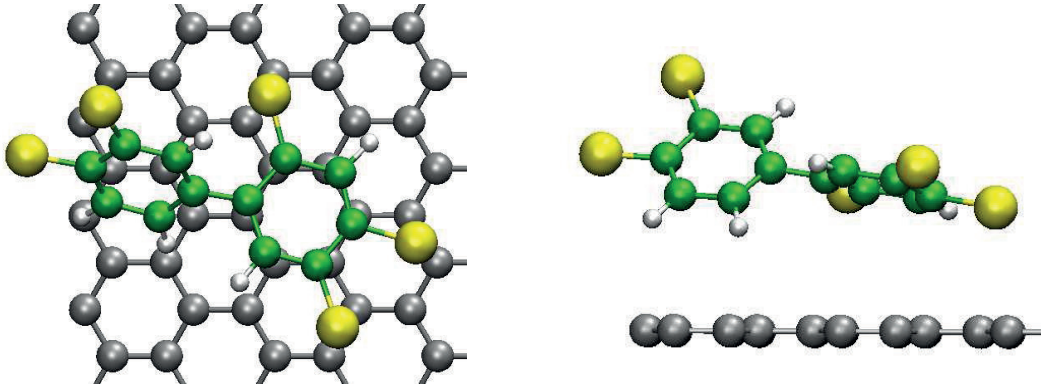

Figure 3: Surface adsorbed PCB congener 118 molecule on top of center pillar in activated carbon model. Note how the aromatic ring has oriented itself on top of the hexagonal structure of activated carbon. It is also interesting to note that on the left figure the hydrogen atoms on the leftmost aromatic ring has oriented themselves over the two negatively charged rows of carbon atoms.

As shown in table 2, the electrostatic interactions are adverse for this orientation. It is, indeed, not making the adsorption more favorable. However, the Lennard-Jones interactions are significantly higher for this orientation, so if the surface had been electrostatic neutral it would certainly have been the most favorable adsorption site. Note that the main contribution that makes this spot favorable comes from the Lennard-Jones interaction with triolein. But it should not be neglected that the Lennard-Jones interaction with the

activated carbon is $\sim 20\ kJ\ mol^{-1}$ lower (more negative) than for that of both PCB congener 77 and 118 adsorbed to pore wall. This is, however, not shown in the tabulated data. In terms of total interaction energies, this positioning is the second least favorable observed. The least favorable positioning was for the pore adsorbed PCB 77 molecule. Interestingly enough, the two most favorable configurations for the molecules are to only be attached to the pore walls via one or two of their chlorine substitutions. Both PCB congeners had in this configuration a significantly lower interaction energy. Basically, they experience an overall favorable interaction with activated carbon and at the same time has most of its surface available to interact with triolein.

5. Conclusions

As discussed above, no significant selectivity was observed during the 4 nanoseconds of our production run. These observations somewhat contradict the experimental results, leading us to conclude that the models employed, especially the activated carbon, need to be refined further. Several potential model shortcomings have been discussed already. Predominantly, we believe that partial atomic charges assigned to the activated carbon bear the main responsibility for the findings. Nevertheless, the current work has succeeded in clarifying some of the key assumptions proposed by the various hypotheses as well as mapping out the future path.

The extent to which the lack of pore wall defects may have affected the system evolution, as well as the impact of pore dimensions is definitely issues that merit a more thorough investigation. As noted earlier, a more irregular structure may favor selective adsorption while being truer to the real-life activated carbon. It might also be beneficial to introduce wedge-like pores instead of plain slit ones. Observations discussed in Section 4.1 appear to indicate that wedge-shaped pores that gradually infer larger steric constraints might contribute to a greater selectivity between different PCB congeners. Considering that the average pore diameter the study conducted by Jonker and Koelmans is 3.0 nm, and that their study indicates a strong positive correlation between the average pore distribution and the distribution coefficient, it is quite possible that smaller pores combined with and a narrow pore distribution might lead to more conclusive results.

We have also found that planar adsorption onto hexagonal activated carbon surface will be heavily favored by the short range interactions and hindered by presence of electrostatic forces. Given that congener 77 is more suit-

able for planar adsorption, its experimentally confirmed selective adsorption would be promoted in case of carbon with neutral rather than substantial partial charges like in our model. Further investigation of this hypothesis may be carried out in a new simplified setup consisting of a single slit pore. Comparing the behavior and selectivity of pores made of neutral graphite sheets with those of pores made of charged carbon atoms, like the ones used in this work, would provide an opportunity to test the basic assumptions of hypotheses under evaluation.

Our preliminary findings led us to believe that the activate carbon selectivity may stem from the combination of pore trapping and planar adsorption. Pores sufficiently small in size will hinder PCB congener 118 from entering due to purely geometric constraints. Their walls will also offer adsorption sites preferentially selective for PCB congener 77 which favor planar conformation and thus is capable of more vigorous short-range interactions. This combination would result in a two-stage selectivity for the PCB congeners 118 and 77. However, since no PCB congener 77 adsorbed on top of a graphite sheet during the production run, no interaction energies could be calculated to either verify or disprove this hypothesis. A comparison from a short, trivial, simulation with a graphite sheet and PCB congener 77 and 118 would shed more light on this and also provide comparable energies.

Acknowledgements

Our thanks to William L. Jorgensen who was kind enough to send the entire set of OPLS parameters upon request. Thanks also go to Bergen Center for Computation Science for use of the cluster, and to Pronova BioPharma, Egersund Sildoljefabrikk, Marine Harvest and the Research Council of Norway (project 178969/S40) for economical support.

References

[1] Å. Oterhals, M. Solvang, R. Nortvedt, M. H. G. Berntssen, Optimization of activated carbon-based decontamination of fish oil by response surface methodology, European Journal of Lipid Science and Technology 109 (7) (2007) 691–705, doi:10.1002/ejlt.200700083.

[2] A.-K. Lundebye, M. Berntssen, Å. Lie, G. Ritchie, P. Isosaari, H. Kiviranta, T. Vartiainen, Dietary uptake of dioxins (PCDD/PCDFs) and

dioxin-like PCBs in Atlantic salmon (Salmo salar), Aquaculture Nutrition 10 (3) (2004) 199–207, doi:0.1111/j.1365-2095.2004.00299.x.

[3] R. A. Hites, J. A. Foran, D. O. Carpenter, M. C. Hamilton, e. al., Global Assessment of Organic Contaminants in Farmed Salmon, Science 303 (5655).

[4] A. Oterhals, E. Nygard, Reduction of persistent organic pollutants in fishmeal: A feasibility study, Journal of Agricultural and Food Chemistry 56 (6) (2008) 2012–2020, doi:10.1021/Jf072883k.

[5] Y. Guo, S. Kaplan, T. Karanfil, The significance of physical factors on the adsorption of polyaromatic compounds by activated carbons, Carbon 46 (2008) 1885–1891.

[6] M. T. O. Jonker, F. Smedes, Preferential Sorption of Planar Contaminants in Sediments from Lake Ketelmeer, The Netherlands, Environ. Sci. Technol. 34 (2000) 1620–1626.

[7] M. T. O. Jonker, A. A. Koelmans, Sorption of Polycyclic Aromatic Hydrocarbons and Polychlorinated Biphenyls to Soot and Soot-like Materials in the Aqueous Environment: Mechanistic Considerations, Environ. Sci. Technol. 36 (2002) 3725–3734.

[8] T. D. Bucheli, G. Örjan, Soot sorption of non-*ortho* and *ortho* substituted PCBs, Chemosphere 53 (2003) 515–522.

[9] T. J. Barton, L. M. Bull, W. G. Klemperer, D. A. Loy, B. McEnaney, M. Misono, P. A. Monson, G. Pez, G. W. Scherer, J. C. Vartuli, O. M. Yaghi, Tailored porous materials, Chemistry of Materials 11 (10) (1999) 2633–2656, doi:10.1021/cm9805929.

[10] R. C. Bansal, M. Goyal, Activated carbon adsorption, Taylor & Francis, Boca Raton, La. ; London, 2005.

[11] T. D. Bucheli, G. Örjan, Quantification of the Soot-Water Distribution Coefficient of PAHs Provides Mechanistic Basis for Enhanced Sorption Observations, Environ. Sci. Technol. 34 (2000) 5144–5151.

[12] P. Laakso, W. W. Christie, J. Pettersen, Analysis of North-Atlantic and Baltic Fish Oil Triacylglycerols by High-Performance Liquid-Chromatography with a Silver Ion Column, Lipids 25 (5) (1990) 284–291.

[13] W. L. Jorgensen, D. S. Maxwell, J. TiradoRives, Development and testing of the OPLS all-atom force field on conformational energetics and properties of organic liquids, Journal of the American Chemical Society 118 (45) (1996) 11225–11236.

[14] W. Damm, A. Frontera, J. TiradoRives, W. L. Jorgensen, OPLS all-atom force field for carbohydrates, Journal of Computational Chemistry 18 (16) (1997) 1955–1970.

[15] W. L. Jorgensen, N. A. McDonald, Development of an all-atom force field for heterocycles. Properties of liquid pyridine and diazenes, Theochem-Journal of Molecular Structure 424 (1-2) (1998) 145–155.

[16] N. A. McDonald, W. L. Jorgensen, Development of an all-atom force field for heterocycles. Properties of liquid pyrrole, furan, diazoles, and oxazoles, Journal of Physical Chemistry B 102 (41) (1998) 8049–8059.

[17] R. C. Rizzo, W. L. Jorgensen, OPLS all-atom model for amines: Resolution of the amine hydration problem, Journal of the American Chemical Society 121 (20) (1999) 4827–4836.

[18] M. L. P. Price, D. Ostrovsky, W. L. Jorgensen, Gas-phase and liquid-state properties of esters, nitriles, and nitro compounds with the OPLS-AA force field, Journal of Computational Chemistry 22 (13) (2001) 1340–1352.

[19] E. K. Watkins, W. L. Jorgensen, Perfluoroalkanes: Conformational analysis and liquid-state properties from ab initio and Monte Carlo calculations, Journal of Physical Chemistry A 105 (16) (2001) 4118–4125.

[20] W. L. Jorgensen, J. P. Ulmschneider, J. Tirado-Rives, Free energies of hydration from a generalized Born model and an ALL-atom force field, Journal of Physical Chemistry B 108 (41) (2004) 16264–16270.

[21] K. P. Jensen, W. L. Jorgensen, Halide, ammonium, and alkali metal ion parameters for modeling aqueous solutions, Journal of Chemical Theory and Computation 2 (6) (2006) 1499–1509, doi:10.1021/Ct600252r.

[22] Schrödinger LLC Jaguar v7.5, 2008.

[23] A. Becke, Density-Functional Thermochemistry .3. The Role of Exact Exchange, Journal of Chemical Physics 98 (7) (1993) 5648–5652, ISSN 0021-9606.

[24] P. J. Stephens, F. J. Devlin, C. F. Chabalowski, M. J. Frisch, Ab Initio Calculation of Vibrational Absorption and Circular Dichroism Spectra Using Density Functional Force Fields, The Journal of Physical Chemistry 98 (45) (1994) 11623–11627, doi:10.1021/j100096a001, URL http://pubs.acs.org/doi/abs/10.1021/j100096a001.

[25] M. Jorge, N. A. Seaton, Long-range interactions in Monte Carlo simulation of confined water, Molecular Physics 100 (13) (2002) 2017–2023.

[26] A. V. OShevade, S. Jiang, K. E. Gubbins, Molecular simulation study of water-methanol mixtures in activated carbon pores, J. Chem. Phys. 113 (2000) 6933–6943, doi:10.1063/1.1309012.

[27] C. Tenney, C. Lastoskie, Molecular Simulation of Carbon Dioxide Adsorption in Chemically and Structurally Heterogeneous Porous Carbons, Environmental Progress 25 (4) (2007) 343–354, doi:10.1002/ejlt.200700083.

[28] C. P. Kelly, C. J. Cramer, D. G. Truhlar, SM6: A density functional theory continuum solvation model for calculating aqueous solvation free energies of neutrals, ions, and solute-water clusters, Journal of Chemical Theory and Computation 1 (6) (2005) 1133–1152, doi:10.1021/Ct050164b.

[29] R. M. Olson, A. V. Marenich, C. J. Cramer, D. G. Trublarlc, Charge model 4 and intramolecular charge polarization, Journal of Chemical Theory and Computation 3 (6) (2007) 2046–2054, doi:10.1021/ct7001607.

[30] J. D. Thompson, J. D. Xidos, T. M. Sonbuchner, C. J. Cramer, D. G. Truhlar, More reliable partial atomic charges when using diffuse basis sets, Physchemcomm (2002) 117–134doi:10.1039/B206369g.

[31] A. P. Lyubartsev, A. Laaksonen, MDynaMix - a scalable portable parallel MD simulation package for arbitrary molecular mixtures, Computer Physics Communications 128 (3) (2000) 565–589.

[32] A. P. Lyubartsev, A. Laaksonen, MDynaMix Homepage, URL `http://www.fos.su.se/~sasha/mdynamix/`, 2010.

[33] W. Humphrey, A. Dalke, K. Schulten, VMD – Visual Molecular Dynamics, Journal of Molecular Graphics 14 (1996) 33–38.

[34] S. Nose, A Unified Formulation of the Constant Temperature Molecular-Dynamics Methods, Journal of Chemical Physics 81 (1) (1984) 511–519.

[35] S. Nose, A Molecular-Dynamics Method for Simulations in the Canonical Ensemble, Molecular Physics 52 (2) (1984) 255–268.

[36] W. G. Hoover, Canonical dynamics: Equilibrium phase-space distributions, Physical Review A 31 (Copyright (C) 2009 The American Physical Society) (1985) 1695, URL `http://link.aps.org/abstract/PRA/v31/p1695`.

[37] D. Simmons, A. Chauhan, Influence of physical and chemical heterogeneity shape on thin film rupture, Journal of Colloid and Interface Science 295 (2) (2006) 472 – 481, ISSN 0021-9797, doi:DOI: 10.1016/j.jcis.2005.09.009.

[38] F. Barberis, G. Cama, M. Capurro, E. Finocchio, Liquid-solid nanointeractions of ceramic and metals, in: Nanotechnology, 2009. IEEE-NANO 2009. 9th IEEE Conference on, ISSN 1944-9399, 355 –358, 2009.

[39] F. W. Starr, J. K. Nielsen, H. E. Stanley, Fast and Slow Dynamics of Hydrogen Bonds in Liquid Water, Phys. Rev. Lett. 82 (11) (1999) 2294–2297, doi:10.1103/PhysRevLett.82.2294.